# Discontinuity-Driven Mesh Alignment for Evolving Discontinuities in Elastic Solids

Mihhail Berezovski*

*Department of Mathematics, Embry-Riddle Aeronautical University, FL, USA*

Arkadi Berezovski

*Department of Cybernetics, School of Science, Tallinn University of Technology, Tallinn, Estonia*

**Abstract**

A special mesh adaptation technique and a precise discontinuity tracking are presented for an accurate, efficient, and robust adaptive-mesh computational procedure for one-dimensional hyperbolic systems of conservation laws, with particular reference to problems with evolving discontinuities in solids. The main advantage of the adaptive technique is its ability to preserve the modified mesh as close to the original fixed mesh as possible. The constructed method is applied to the martensitic phase-transition front propagation in solids.

*Keywords:* Mesh alignment, Evolving discontinuities, Elastic solids, Conservation laws, Martensitic phase transition

*2010 MSC:* 74A60, 74E05, 74J05

## 1. Introduction

The paper contributes to the solution of the long-term problem of the tracking of moving discontinuities in solids by means of the reallocation of a deformable mesh, as well as to the prediction of the evolution of unavoidable discontinuities.

*Corresponding author

*Email addresses:* mihhail.berezovski@gmail.com (Mihhail Berezovski), arkadi.berezovski@cs.ioc.ee (Arkadi Berezovski)

Heterogeneity is a typical feature of solids and structures. Distinct homogeneous parts of a material (layers, inclusions, grains, etc.) are divided from one another by boundaries or interfaces. Theoretically, such sharp interfaces can be idealized as discontinuities. Among them, evolving discontinuities hold a specific place due to their theoretical complexity and practical importance. Location of such discontinuities is not prescribed in advance. It varies in time and space under external loading. The most known examples of evolving discontinuities in solid mechanics are brittle cracks and martensitic phase-transition fronts.

Dynamics of such discontinuities is determined by two factors, that is, by the driving force acting at the discontinuity and by the velocity of the discontinuity. Both the driving force and the velocity of discontinuity have been subjects of intensive research in the case of martensitic phase transition fronts [1] and brittle crack dynamics [2, 3]. The driving force acting at discontinuity is a specific example of the well-established concept of configurational forces [4–6]. It can be calculated by means of standard numerical methods. The question about the velocity of a discontinuity is more subtle. In contrast to gas dynamics, where the velocity of shock wave can be calculated by means of the Rankine-Hugoniot jump relations [7], macroscopic jump conditions in solid mechanics do not provide enough information, for instance, to specify the velocity of a phase boundary uniquely. Uniqueness of the solution can be achieved by the introduction of two supplementary constitutive-like relationships: a kinetic law for a driving force that establishes the speed of the phase transformation front and a nucleation criterion [1]. The constitutive theory of kinetic relations is not completely established yet.

It is well known [8, e.g.] that even if we know the values of the driving force and the velocity of a discontinuity, this does not guarantee a precise description of the motion of the discontinuity using numerical methods. The necessary precision can be achieved only if the location of the discontinuity coincides with a mesh node at each time step. The accuracy in the determination of velocity and location of the discontinuity is crucial. An error in the location of

the discontinuity leads to an incorrect distribution of field values which results in an improper value of the driving force acting at the discontinuity. Then the divergence from the true solution will increase more and more up to undesired values. This means that the location of the discontinuity should be as precise as possible. Such a requirement demands mesh alignment with discontinuity.

Mesh adaptation is not a new idea. Various methods employ a non-uniform mesh that is sparse in regions where the solution is smooth and more concentrated near discontinuities [9], or use the refinement of the grid by splitting computational cells near discontinuity [10]. However, the distortion of an adapted mesh can be too large [11], which may result in inadequacy of the solution. Another approach is to track the discontinuity by virtue of a locally distorted mesh allowing the discontinuity to jump from one computational cell to another [8]. In this case, the local re-meshing of two cells adjacent to a discontinuity may produce an inappropriate distortion.

Let us consider the results of numerical simulation of the martensitic phase boundary motion in the problem formulated in Section 4 using two different methods of the front tracking following Zhong et al. [8] and Fazio and LeVeque [11]. It should be noted that these calculations are performed by means of the wave propagation algorithm [12] under identical conditions specified in Section 4 and using the same kinetic relation. The results of the calculations are presented in Fig. 1.

As one can see, the prediction of the front propagation diverges substantially depending on the front tracking procedure. Moreover, if the mesh size is changed (say, increased in two times), then the results in both cases are changed significantly. The difference in results for the method by Zhong et al. [8] is shown in Fig. 2. Even more drastically difference is observed for the method of capacity function [11], as one can see in Fig. 3.

These examples manifest the necessity of the accuracy in the determination of velocity and location of the discontinuity.

The discontinuity-driven mesh adaptation presented in the paper is the synthesis of the moving mesh approach [11] with an appropriate ”capacity

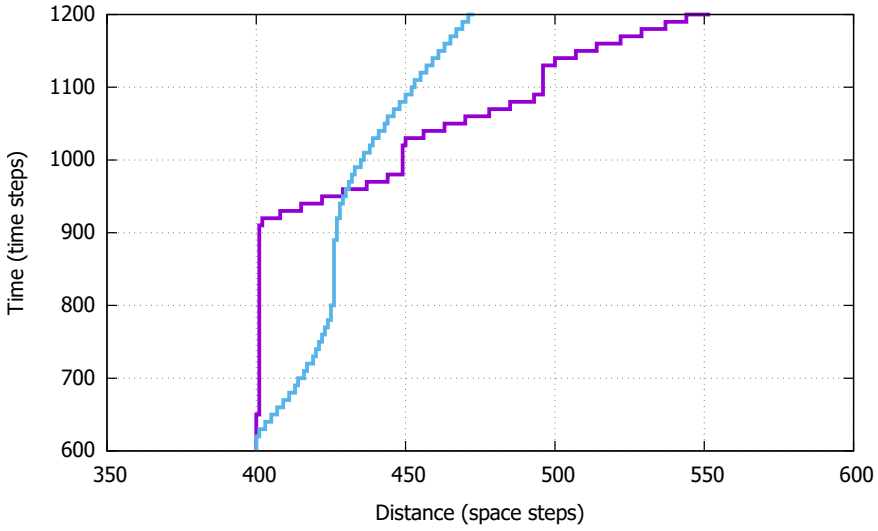


Figure 1: Predictions of a martensitic front propagation for Ni-Ti shape memory alloy under impact loading. Blue line corresponds to the location of the front position by means of capacity function [11], magenta line represents the front position according to the reallocation procedure [8].

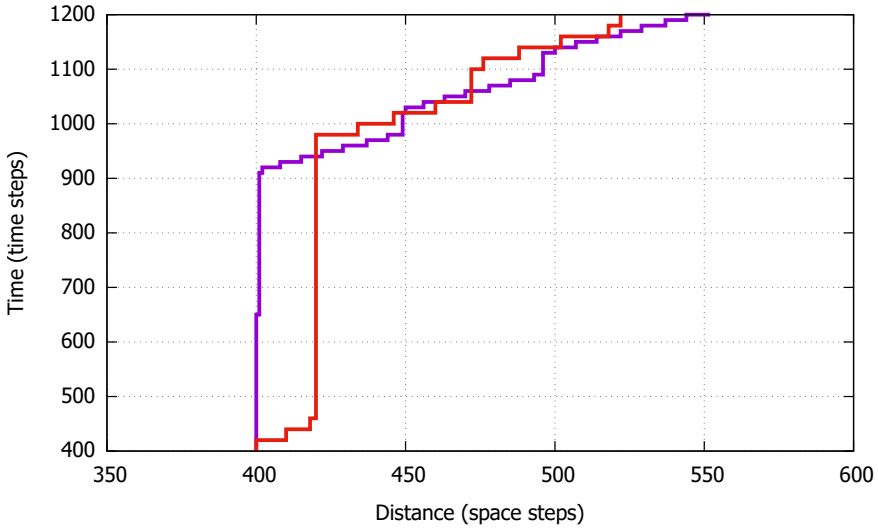


Figure 2: Predictions of a martensitic front propagation according to the reallocation procedure [8]. Here magenta line is the same as in Fig. 1 and red line corresponds to the coarse mesh.

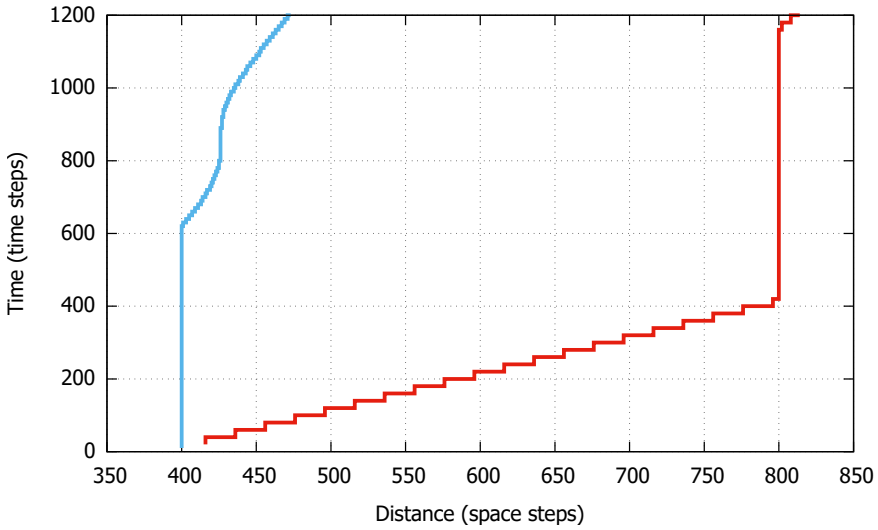


Figure 3: Predictions of a martensitic front propagation according to [11]. The blue line is the same as in Fig. 1 and red line corresponds to the coarse mesh.

function" [12] and a reallocation technique similar to proposed in [8]. Such a combination of the two approaches preserves the advantages of both. Additionally, the algorithmic computation of the velocity of discontinuity [13] is applied.

The moving mesh technique is described in Section 2 including grid mapping and alignment. As an example, martensitic phase-transition front propagation problem is reminded in Section 3. The difference between the location of a discontinuity with and without mesh alignment is demonstrated in Section 4. Conclusions and discussion are presented in the last Section.

## 2. Mesh alignment

### *2.1. Conservation laws*

Wave motion in elastic solids is governed by the balance of linear momentum, the kinematic compatibility conditions, and the Hooke law. In one space dimension the governing equations can be written the form of conservation

laws [14, 15]

$$\frac{\partial}{\partial t}\mathbf{q}(x,t) + \frac{\partial}{\partial x} f(\mathbf{q}(x,t)) = 0, \tag{1}$$

where $t$ is time, $x$ is space variable, $\mathbf{q}$ is a vector of conserved quantities, and $f(\mathbf{q})$ is called the flux function.

Let us introduce a computational grid of cells $C_n = [x_i, x_{i+1}]$ with interfaces $x_i = i\Delta x$ and time levels $t_k = k\Delta t$. For simplicity, the grid size $\Delta x$ and time step $\Delta t$ are assumed to be constant. It should be noted that we set the index $n$ for cell description and keep boundaries of $n$th cell as $x_i$ and $x_{i+1}$ for later convenience. Then we introduce the average $\bar{\mathbf{q}}_n^k$ of the exact solution on $C_n$ at the time instant $t = t_k$

$$\bar{\mathbf{q}}_n^k = \frac{1}{\Delta x}\int_{x_i}^{x_{i+1}} \mathbf{q}(x,t_k)dx. \tag{2}$$

The difference between the value of the quantity $\mathbf{q}(x,t_k)$ and its averaged value $\bar{\mathbf{q}}_n^k$ is represented by so-called excess quantity $Q_n^k(x)$ [13], i.e.,

$$\mathbf{q}(x,t_k) = \bar{\mathbf{q}}_n^k + \mathbf{Q}_n^k(x). \tag{3}$$

It should be noted that the values of excess quantity at the ends of the interval $[x_i, x_{i+1}]$ are only of interest. We denote them as $\mathbf{Q}_n^k(x_i) = (\mathbf{Q}_n^k)^-$ and $\mathbf{Q}_n^k(x_{i+1}) = (\mathbf{Q}_n^k)^+$. For a linear function $f$

$$f(\mathbf{q}(x,t_k)) = f(\bar{\mathbf{q}}_n^k) + f(\mathbf{Q}_n^k(x)), \tag{4}$$

and we can represent the flux function at boundaries of the cell as follows:

$$f(\mathbf{q}(x_i,t_k)) = f(\bar{\mathbf{q}}_n^k) + (\mathbf{F}_n^k)^-, \quad f(\mathbf{q}(x_{i+1},t_k)) = f(\bar{\mathbf{q}}_n^k) + (\mathbf{F}_n^k)^+. \tag{5}$$

Integration the conservation law (1) over the computational cell $n$ gives

$$\begin{aligned} &\frac{\partial}{\partial t}\int_{x_i}^{x_{i+1}} \mathbf{q}(x,t)dx = -f(\mathbf{q}(x_{i+1},t)) + f(\mathbf{q}(x_i,t)) = \\ &= -f(\bar{\mathbf{q}}_n^k) - (\mathbf{F}_n^k)^+ + f(\bar{\mathbf{q}}_n^k) + (\mathbf{F}_n^k)^- = -(\mathbf{F}_n^k)^+ + (\mathbf{F}_n^k)^-. \end{aligned} \tag{6}$$

Using the definition of averaged quantity (2) and applying the standard approximation for the time derivative, we can represent Eq. (6) as a numerical scheme in terms of excess quantities

$$\bar{\mathbf{q}}_n^{k+1} = \bar{\mathbf{q}}_n^k - \frac{\Delta t}{\Delta x}\left((\mathbf{F}_n^k)^+ - (\mathbf{F}_n^k)^-\right). \tag{7}$$

Comparing with flux-differencing scheme [14], we can see that here the excess quantities are used instead of numerical fluxes. This scheme is working well on fixed mesh [13] and has the same properties of accuracy and stability as those established for the conservative wave propagation algorithm [16].

### 2.2. *Moving mesh*

Keeping in mind a possible motion of a discontinuity, we set a moving mesh. We suppose that the computational domain is alternatively divided using a set of points which move in time and are parameterized by $z_i^k = z(x_i, t_k)$. We keep the original fixed mesh as a part of the adaptive technique, i.e., $z_i^0 = x_i$. Following [11], we assume that the motion of points $z_i$ has a constant speed

$$\dot{z}_i^k = \frac{z_i^{k+1} - z_i^k}{\Delta t}, \tag{8}$$

over each time step $[t_k, t_{k+1}]$. The transfer from the fixed mesh to the moving mesh is illustrated in Fig. 4.

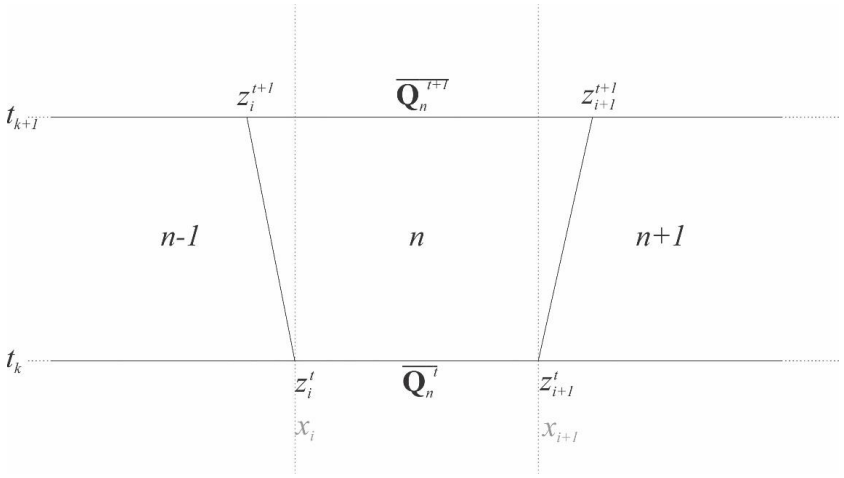


Figure 4: Moving mesh.

As it is demonstrated in [11], the dependence $\tilde{\mathbf{q}}(x,t) \equiv \mathbf{q}(z(x,t),t)$ transforms conservation laws (1) into

$$(z_x \tilde{\mathbf{q}})_t + (f(\tilde{\mathbf{q}}) - z_t \tilde{\mathbf{q}})_x = 0. \tag{9}$$

Integration of conservation law (9) over the undistorted cell now results in

$$\begin{aligned}&\frac{\partial}{\partial t}(\Delta z_n \bar{\mathbf{q}}_n^k) + (\mathbf{F}_n^k)^+ - (\mathbf{F}_n^k)^- - \\ &- \dot{z}_{i+1}^k(\bar{\mathbf{q}}_n^k + (\mathbf{Q}_n^k)^+) + \dot{z}_i^k(\bar{\mathbf{q}}_n^k + (\mathbf{Q}_n^k)^-) = 0.\end{aligned} \tag{10}$$

Applying the standard approximation for the time derivative and defining the capacity $\kappa_n^k = \Delta z_n^k / \Delta x$ [11], we represent the obtained relationship as

$$\begin{aligned}\kappa_n^{k+1}\bar{\mathbf{q}}_n^{k+1} - \kappa_n^k \bar{\mathbf{q}}_n^k = -\frac{\Delta t}{\Delta x}\left[(\mathbf{F}_n^k)^+ - (\mathbf{F}_n^k)^-\right] + \\ + \frac{\Delta t}{\Delta x}\left[\dot{z}_{i+1}^k(\bar{\mathbf{q}}_n^k + (\mathbf{Q}_n^k)^+) - \dot{z}_i^k(\bar{\mathbf{q}}_n^k + (\mathbf{Q}_n^k)^-)\right].\end{aligned} \tag{11}$$

The final form of the numerical scheme in terms of excess quantities

$$\kappa_n^{k+1}\bar{\mathbf{q}}_n^{k+1} = \kappa_n^{k+1}\bar{\mathbf{q}}_n^k - \frac{\Delta t}{\Delta x}\left[(\mathbf{F}_n^k)^+ - \dot{z}_{i+1}^k(\mathbf{Q}_n^k)^+ - (\mathbf{F}_n^k)^- + \dot{z}_i^k(\mathbf{Q}_n^k)^-\right], \tag{12}$$

follows by the use of the observation [11]

$$\kappa_n^k \bar{\mathbf{q}}_n^k = \kappa_n^{k+1}\bar{\mathbf{q}}_n^k - \frac{\Delta t}{\Delta x}\left[\dot{z}_{i+1}^k - \dot{z}_i^k\right]\bar{\mathbf{q}}_n^k. \tag{13}$$

As shown in [17], it is convenient to represent numerical scheme (12) in the wave propagation form

$$\kappa_n^{k+1}\bar{\mathbf{q}}_n^{k+1} = \kappa_n^{k+1}\bar{\mathbf{q}}_n^k - \frac{\Delta t}{\Delta x}\left[(\mathbf{F}_n^k)^+ - (\mathbf{F}_n^k)^-\right], \tag{14}$$

determining values of excess quantities at the boundaries of computational cells by means of jump relations (for each cell $n$ and time step $k$)

$$[\![f(\bar{\mathbf{q}}) + \mathbf{F} + \dot{z}_i(\bar{\mathbf{q}} + \mathbf{Q})]\!] = 0. \tag{15}$$

Here $[\![A]\!] = A^+ - A^-$, and $A^\pm$ are uniform limits of a field $A$ in approaching the boundary from its positive and negative sides, respectively.

The numerical form of the jump relations is then

$$\begin{aligned}&(\mathbf{F}_n^k)^- - (\mathbf{F}_{n-1}^k)^+ - \dot{z}_i^k\left[(\mathbf{Q}_n^k)^- - (\mathbf{Q}_{n-1}^k)^+\right] = \\ &= -(f(\bar{\mathbf{q}}_n^k) - f(\bar{\mathbf{q}}_{n-1}^k) + \dot{z}_i^k(\bar{\mathbf{q}}_n^k - \bar{\mathbf{q}}_{n-1}^k).\end{aligned} \tag{16}$$

The major advantage of using this type of formulation is a natural way in which the mesh motion is incorporated into discrete equations. This is contrasted with methods that explicitly introduce terms of the form $\dot{z}_i^k \bar{\mathbf{q}}_n^k$ into numerical scheme, which can lead to problems with stability [18].

*2.3. Grid mapping*

Now we will introduce a specific grid mapping function in order not to fix the grid point attached to the discontinuity but to determine the closest grid point to the location of the discontinuity at each time step. Instead of the reallocation for only a limited number of shifted cells as in [8], it will be applied on whole computational domain that reduces the distortion of the grid.

The computational domain is discretized in such a way that the discontinuity is always at an interface between computational cells. If at a time instant $t_k$ the discontinuity is located at a certain cell interface, then the computation will proceed as follows:

- Compute all quantities at the time instant $t_{k+1}$ from the known state at the time instant $t_k$, including the discontinuity propagation speed, and then the location of the discontinuity at $t_{k+1}$.
- Calculate the grid mapping function according to the movement of the discontinuity so that the discontinuity is still at a cell interface.
- Update all quantities at the time instant $t_{k+1}$ for the adapted mesh.

Assume that the position of the discontinuity $G$ is known at time $t = t_k$

$$G(t_k) = G^k. \tag{17}$$

If the velocity of the propagation of the discontinuity $v_g^k$ is determined, then we can calculate the position of the discontinuity at the next time step

$$G^{k+1} = G^k + v_g^k \Delta t. \tag{18}$$

Then we can choose the fixed grid cell boundary $\hat{G}_x^{k+1}$, which is the closest to the updated front location simply checking the relation

$$|G^{k+1} - \hat{G_x}^{k+1}| < \frac{\Delta x}{2}. \tag{19}$$

The grid mapping for moving mesh coordinates is given by

$$z_i^{k+1} = \begin{cases} \frac{1}{\hat{G}_x^{k+1} - a}(x_i - a)G^{k+1}, & a \le x_i \le G^{k+1} \\ G^{k+1} + \frac{1}{b - \hat{G}_x^{k+1}}(x_i - \hat{G}_x^k)(b - G^{k+1}), & G^{k+1} < x_i < b. \end{cases} \tag{20}$$

The explicit positioning of the discontinuity ensures the calculation of averaged quantities using the values belonging to only one side of the discontinuity (a front side or a rear side). This supports the stability of computations and prevent unphysical damping.

The proposed technique is illustrated on the example of one-dimensional martensitic phase-transition front propagation in the next Section.

## 3. Example: Martensitic phase-transition front propagation

The simplest example of an evolving discontinuity in elastic solids is a stress-induced phase-transition front between martensite and austenite phases in a shape memory material, because its continuum description can be considered in one-dimensional setting [1]. The formulation of the stress-induced phase-transition front propagation problem is given in the case of an isothermal uniaxial motion of a bar with a unit cross-section. The bar occupies the interval $0 < x < L$ in a reference configuration and assumed to be longer than its diameter so it is under uniaxial stress state and the stress $\sigma(x,t)$ depends only on the axial position and time. The density of the material $\rho$ is assumed to be constant.

Strain and velocity fields are connected to the displacement $u(x,t)$ of a point $x$ at time $t$

$$\varepsilon(x,t) = \frac{\partial u}{\partial x}, \quad v(x,t) = \frac{\partial u}{\partial t}, \tag{21}$$

respectively. The strain $\varepsilon(x,t)$ suffers discontinuity jump across a phase boundary. The displacement field is assumed to remain continuous throughout the bar. The balance of linear momentum and kinematic compatibility require that away from a phase boundary

$$\rho \frac{\partial v}{\partial t} = \frac{\partial \sigma}{\partial x}, \tag{22}$$

$$\frac{\partial \varepsilon}{\partial t} = \frac{\partial v}{\partial x}, \tag{23}$$

where the function $\sigma(\varepsilon)$ specifies the stress-strain relation.

The velocity and strain fields subject to the following initial and boundary conditions:

$$\varepsilon(x,0) = v(x,0) = 0, \qquad \text{for} \quad 0 < x < L, \tag{24}$$

$$v(0,t) = v_0(t), \quad \varepsilon(L,t) = 0, \quad \text{for} \quad t > 0, \tag{25}$$

where $v_0(t)$ is a given time-dependent function.

On the discontinuity **S** the balance laws reduce to the Rankine-Hugoniot jump conditions

$$V[\![\varepsilon]\!] + [\![v]\!] = 0, \tag{26}$$

$$V[\![\rho v]\!] + [\![\sigma]\!] = 0, \tag{27}$$

where $V$ denotes the velocity of an isolated strain discontinuity **S** which propagates along the bar.

As it is well known, the strain discontinuity that occurs across a propagating phase boundary is a source of dissipation [1], i.e., the martensitic phase transformation is accompanied by an entropy production.

The entropy production is determined by the product of the driving force at the discontinuity and its velocity [6, 19]

$$f_{\mathbf{S}} V \geq 0, \tag{28}$$

where the associated configurational driving force is calculated as follows:

$$f_{\mathbf{S}} = -[\![W]\!] + \langle\sigma\rangle[\![\varepsilon]\!]. \tag{29}$$

Here $W$ is free energy per unit volume and $\langle\sigma\rangle = (\sigma^+ + \sigma^-)/2$.

Unfortunately, the jump relations (26), (27) do not provide enough information to specify the velocity of the phase boundary $V$ uniquely. The only possibility is to use the relationship

$$V^2 = \frac{[\![\sigma]\!]}{\rho[\![\varepsilon]\!]}, \tag{30}$$

which follows from jump relations (26) and (27) since the density $\rho$ is constant in the considered case. However, it is possible only *after* the determination of

the stress (or strain) jump at the discontinuity. Fortunately, the stress jump can be accurately determined algorithmically using the thermodynamically consistent version of the wave propagation algorithm [13] as one can see below.

### 3.1. *Averaged and excess quantities*

In the case of elasticity, averaged and excess quantities are introduced as follows:

$$\sigma = \bar{\sigma} + \Sigma \qquad v = \bar{v} + \mathcal{V}. \tag{31}$$

Here overbars still denote averaged quantity and $\Sigma$ and $\mathcal{V}$ are the corresponding excess quantities. Accordingly, the numerical scheme (7) in terms of excess quantities has the form (c.f. [20])

$$(\overline{\rho v})_n^{k+1} - (\overline{\rho v})_n^k = \frac{\Delta t}{\Delta x}\left((\Sigma_n^k)^+ - (\Sigma_n^k)^-\right), \tag{32}$$

$$\bar{\varepsilon}_n^{k+1} - \bar{\varepsilon}_n^k = \frac{\Delta t}{\Delta x}\left((\mathcal{V}_n^k)^+ - (\mathcal{V}_n^k)^-\right). \tag{33}$$

The boundaries between computational cells represent regular material points and therefore the total stress should be continuous across the boundary between cells

$$[[\bar{\sigma} + \Sigma]] = 0. \tag{34}$$

The jump relation following from the kinematic compatibility reads

$$[[\bar{v} + \mathcal{V}]] = 0. \tag{35}$$

The numerical form of jump relations (34) and (35) is the following:

$$(\Sigma_{n-1}^k)^+ - (\Sigma_n^k)^- = \bar{\sigma}_n^k - \bar{\sigma}_{n-1}^k, \tag{36}$$

$$(\mathcal{V}_{n-1}^k)^+ - (\mathcal{V}_n^k)^- = \bar{v}_n^k - \bar{v}_{n-1}^k. \tag{37}$$

It should be noted that values of excess stresses and excess velocities at the boundaries between computational cells are not independent. They are connected due to the conservation of Riemann invariants [21]

$$\rho_n c_n (\mathcal{V}_n^k)^- + (\Sigma_n^k)^- \equiv 0, \tag{38}$$

$$\rho_{n-1}c_{n-1}(\mathcal{V}^k_{n-1})^+ - (\Sigma^k_{n-1})^+ \equiv 0, \tag{39}$$

where $c$ denotes the velocity of elastic wave.

The system of linear equations (36)-(39) can be solved exactly for each boundary between computational cells determining the values of excess quantities. Then the field quantities can be updated for the next time step by means of numerical scheme (32)-(33). As it was demonstrated [13], the numerical scheme described above is identical to the wave propagation algorithm proposed by LeVeque [12, 14] for smooth solutions. This means that the convergence and accuracy of this scheme are established there.

### 3.2. *Excess quantities at the phase boundary*

The values of excess stresses at the moving phase boundary satisfy the continuity of excess stresses across the phase boundary [13, 19]

$$[[\Sigma]] = 0, \tag{40}$$

which results in

$$\left(\Sigma^k_{p-1}\right)^+ - \left(\Sigma^k_p\right)^- = 0, \tag{41}$$

if the phase boundary is placed between elements $(p-1)$ and $(p)$.

Jump relation (40) expresses the *conservation of the genuine jump at the phase boundary* in the numerical calculations [13] since Eq. (40) yields

$$[[\sigma]] = [[\bar{\sigma} + \Sigma]] = [[\bar{\sigma}]]. \tag{42}$$

Consistently, the conservation of the genuine jump for velocity is also required

$$[[\mathcal{V}]] = 0. \tag{43}$$

Keeping the relations between excess stresses and excess velocities (38), (39) we obtain

$$\frac{(\Sigma^k_{p-1})^+}{\rho_{p-1}c_{p-1}} + \frac{(\Sigma^k_p)^-}{\rho_p c_p} = 0. \tag{44}$$

Conditions (41) and (44) determine vanishing of values of excess stresses at the phase boundary

$$(\Sigma^k_{p-1})^+ = (\Sigma^k_p)^- = 0. \tag{45}$$

Similarly, due to conservation of Riemann invariants (38), (39)

$$(\mathcal{V}_{p-1}^k)^+ = (\mathcal{V}_p^k)^- = 0. \tag{46}$$

Now we can update the state of elements adjacent to the phase boundary since all the excess quantities at the phase boundary are determined. Moreover, we can apply now relationship (30) for the determination of the velocity of the phase boundary. The direction of the front propagation is determined by the positivity of entropy production (28). This algorithmic approach to compute the velocity of a discontinuity was implemented successfully for calculations of martensitic phase-transition front propagation [13]. However, it has been realized only for the fixed mesh. In what follows, the computation of the velocity of a discontinuity is applied in the case of the mesh reallocation.

## 4. Results of numerical simulations

The goal of the simulations is to analyze the phase-transition front propagation under dynamic loading. The phase-transition front is represented by a discontinuity surface of zero thickness separating the different homogeneous austenite and martensite phases. For the considered one-dimensional case, simulations were performed for a bar of the length 25 $cm$ at the temperature 37 $^oC$. Material properties for Ni-Ti shape memory alloy were extracted from [22], where all the details of the experimental procedure are well explained. The Young's moduli are 62 GPa and 22 GPa for austenite and martensite phases, respectively, Poisson's ratio is the same for both phases and is equal to 0.33, the density for both phases is 6450 $kg/m^3$.

The bar is loaded by a step-wise stress pulse from one end. Another end of the bar is fixed. Initially, the bar is at rest. After loading, the phase boundary located initially at some position inside the bar may start to move if the magnitude of the applied stress is high enough.

First, the simulation of the phase transition front propagation is performed in the case of a fixed mesh. The dimensionless computational domain is divided by 1200 space steps with the size of dimensionless space step $\Delta x = 10^{-3}$.

The time step is determined by the requirement for the Courant number to be equal to 1, and therefore, $\Delta t = 10^{-3}$ as well. The initial position of the phase boundary is equal to $400\,\Delta x$. The loading pulse duration is 200 time steps. Its dimensionless magnitude is equal to unity. Calculations are performed for 1200 time steps. The initial and final normalized stress shape is shown in Fig. 5.

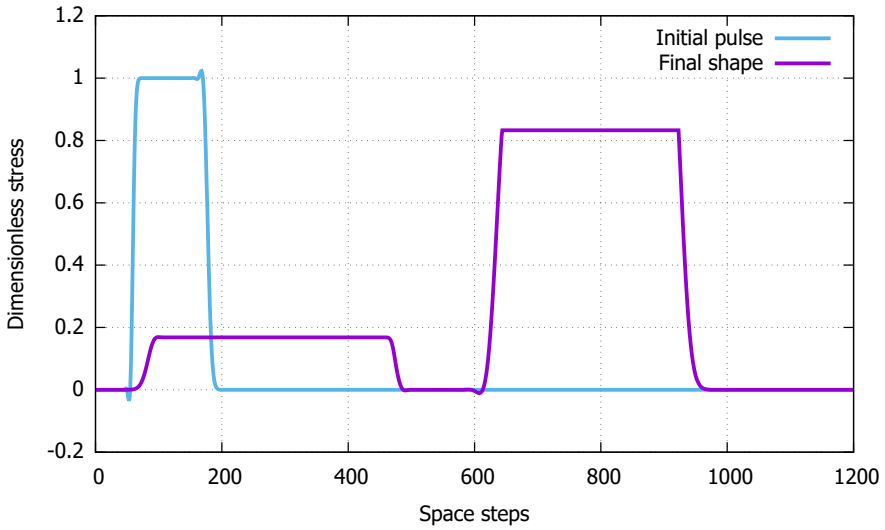


Figure 5: Initial and final stress distribution.

A procedure similar to a cellular automaton is applied to the phase-transition front tracking [13]. At any time step, the values of the driving force are calculated in cells adjacent to the phase boundary. If the value of the driving force at the phase boundary exceeds the critical one, the velocity of the phase front is computed by means of relationship (30). Virtual displacement of the phase-transition front is calculated then for the phase boundary adjacent to the cell. The cell is kept in the old phase state if the virtual displacement is less than the size of the space step, and changes its state to another phase otherwise. The result is represented by the stair-like black line in Fig. 6. Calculations on the coarse mesh are also performed and the result is represented by red line there. As one can see, the dependence on the mesh size is very weak in this case.

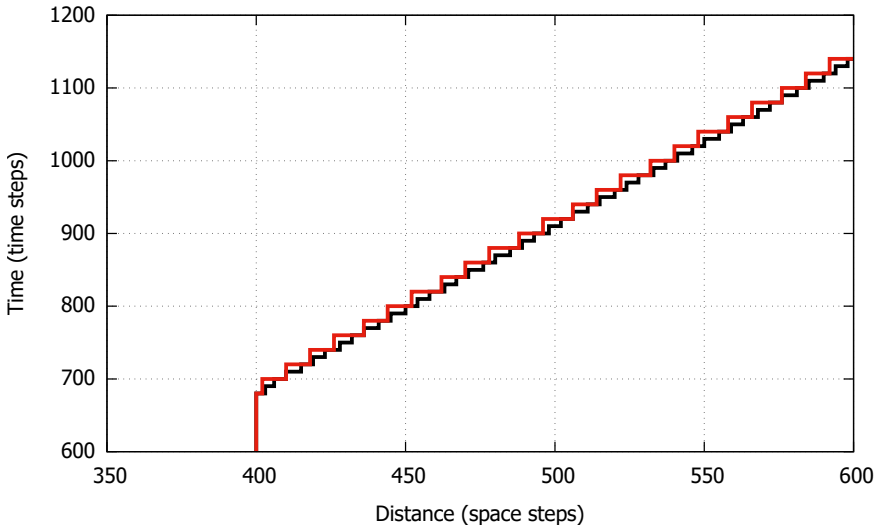


Figure 6: Variation of phase boundary location in time at fixed mesh. Black line represents results of above mentioned method with a fine grid. Red line corresponds to the coarse mesh.

Next, the discontinuity driven mesh adaptation is applied as described in previous sections. The comparison of results with and without reallocation is illustrated in Fig. 7. In this Figure, the black line is the same as in Fig. 6, the blue line displays the results of mesh adaptation and alignment, and red lines show the mesh distortion at every 10 space steps. The mesh distortion looks indiscernible, and it is made more visible in Fig. 8, where a zoomed part of Fig. 7 shows this distortion at every space step.

One can observe a clear distinction in the position of the front obtained by means of adapted and non-adapted mesh. The smooth trajectory of the front position with the mesh adaptation and alignment guarantees the stability of the numerical scheme eliminating the possibility of instabilities due to sudden jumps of the position of the front from one grid point to another which happens if there is no mesh adaptation.

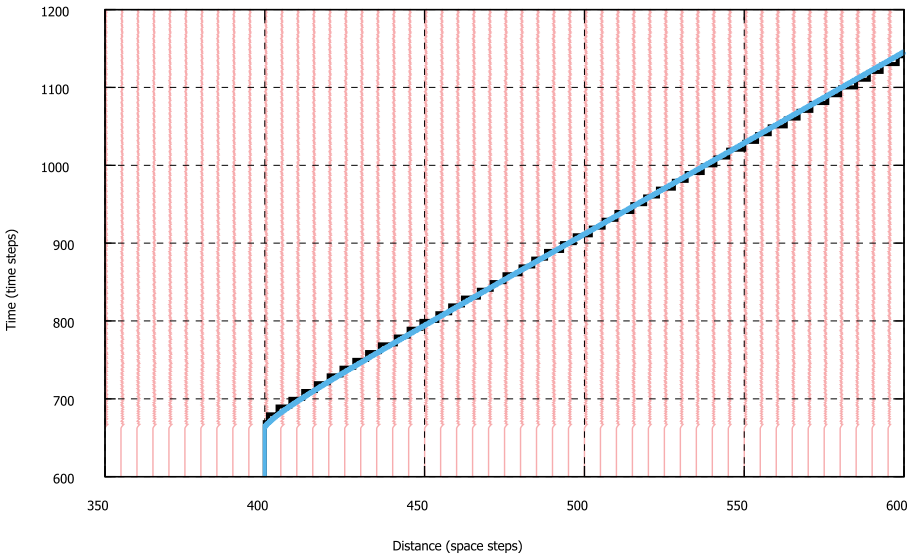


Figure 7: Variation of phase boundary location in time.

## 5. Conclusions and discussion

In the paper, we describe how the discontinuity-driven mesh adaptation procedure for hyperbolic systems of conservation laws can be constructed for problems with moving discontinuities. Key features of the presented method are accuracy and stability, which is ensured by the ability of the adaptive technique to preserve the modified mesh as close to the original fixed one as possible.

It should be noted that there are numerous attempts to achieve an accurate solution of the free boundary problem [23–26], at which jump relations are applied as boundary conditions. The front tracking and front capturing methods are successful only if the velocity of the front can be determined in advance as for shock waves in gas dynamics. This is clearly demonstrated in recent reviews of high-order front tracking and front capturing methods which are presented in [27, 28].

The main difficulty in the corresponding numerical solution is in using grid points on both sides of the discontinuity to approximate a derivative that is

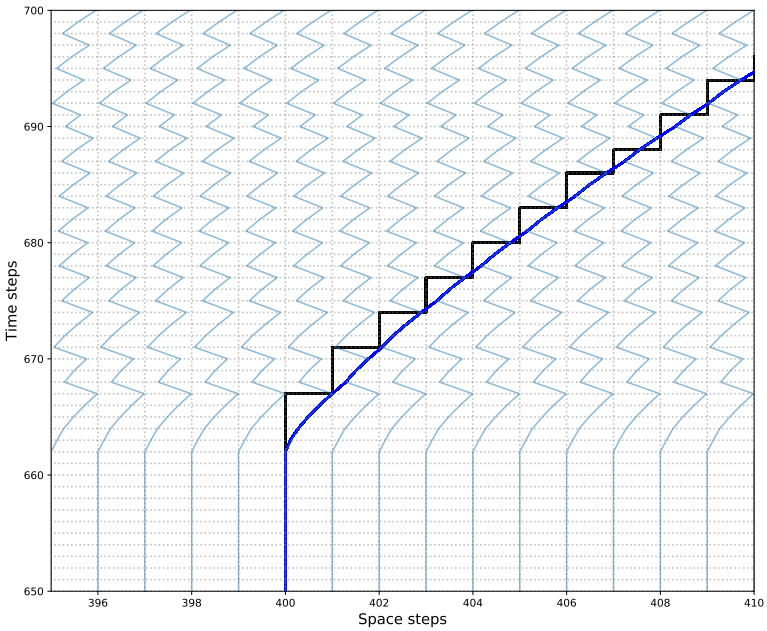


Figure 8: Mesh distortion and phase boundary location in time course.

not even well defined [8]. The only way to determine the velocity of a discontinuity uniquely without an additional constitutive hypothesis is the numerical approach based on the thermodynamically consistent version of the wave propagation algorithm [13]. In this approach, the velocity of the phase boundary is calculated explicitly after the determination of jumps of field quantities at the boundary by means of specific thermodynamic jump conditions. This is why we choose the thermodynamically consistent version of the wave propagation algorithm [13] for the numerical solution of problems with moving discontinuity. It should be noted that on smooth solutions the chosen algorithm is formally identical with the conservative version of the wave propagation algorithm [21]. This means that the accuracy and convergence of the chosen method are the same as in the conservative wave propagation algorithm [16,

e.g.]. As shown on the example of martensitic phase transition front propagation, the method is stable up to the Courant number equal to unity. The extension of the proposed method by a special adaptive dimensional splitting could help to implement this method in higher dimensions. The implementation of this adaptive procedure in higher dimensions is in progress.

**References**


[1] R. Abeyaratne, J. K. Knowles, Evolution of Phase Transitions: A Continuum Theory, Cambridge University Press, 2006.

[2] L. B. Freund, Dynamic Fracture Mechanics, Cambridge University Press, 1990.

[3] K. Ravi-Chandar, Dynamic Fracture, Elsevier, 2004.

[4] G. A. Maugin, Material forces: concepts and applications, Applied Mechanics Reviews 48 (5) (1995) 213–245.

[5] R. Kienzler, G. Herrmann, Mechanics in Material Space: with Applications to Defect and Fracture Mechanics, Springer Science & Business Media, 2000.

[6] G. A. Maugin, Configurational Forces: Thermomechanics, Physics, Mathematics, and Numerics, CRC Press, 2011.

[7] J. M. Hyman, Numerical methods for tracking interfaces, Physica D: Nonlinear Phenomena 12 (1-3) (1984) 396–407.

[8] X. Zhong, T. Y. Hou, P. G. LeFloch, Computational methods for propagating phase boundaries, Journal of Computational Physics 124 (1) (1996) 192–216.

[9] M. J. Berger, R. J. LeVeque, Adaptive mesh refinement using wave-propagation algorithms for hyperbolic systems, SIAM Journal on Numerical Analysis 35 (6) (1998) 2298–2316.

[10] R. J. LeVeque, D. L. George, M. J. Berger, Tsunami modelling with adaptively refined finite volume methods, Acta Numerica 20 (2011) 211–289.

[11] R. Fazio, R. J. LeVeque, Moving-mesh methods for one-dimensional hyperbolic problems using clawpack, Computers & Mathematics with Applications 45 (1-3) (2003) 273–298.

[12] R. J. LeVeque, Wave propagation algorithms for multidimensional hyperbolic systems, Journal of Computational Physics 131 (2) (1997) 327–353.

[13] A. Berezovski, J. Engelbrecht, G. A. Maugin, Numerical Simulation of Waves and Fronts in Inhomogeneous Solids, World Scientific, 2008.

[14] R. J. LeVeque, Finite Volume Methods for Hyperbolic Problems, Vol. 31, Cambridge University Press, 2002.

[15] J. S. Hesthaven, Numerical Methods for Conservation Laws: From Analysis to Algorithms, SIAM, 2018.

[16] D. S. Bale, R. J. LeVeque, S. Mitran, J. A. Rossmanith, A wave propagation method for conservation laws and balance laws with spatially varying flux functions, SIAM Journal on Scientific Computing 24 (3) (2003) 955–978.

[17] J. M. Stockie, J. A. Mackenzie, R. D. Russell, A moving mesh method for one-dimensional hyperbolic conservation laws, SIAM Journal on Scientific Computing 22 (5) (2001) 1791–1813.

[18] S. Li, L. Petzold, Y. Ren, Stability of moving mesh systems of partial differential equations, SIAM Journal on Scientific Computing 20 (2) (1998) 719–738.

[19] A. Berezovski, G. A. Maugin, Jump conditions and kinetic relations at moving discontinuities, ZAMM-Journal of Applied Mathematics and Mechanics/Zeitschrift für Angewandte Mathematik und Mechanik 90 (7-8) (2010) 537–543.

[20] A. Berezovski, G. Maugin, Simulation of thermoelastic wave propagation by means of a composite wave-propagation algorithm, Journal of Computational Physics 168 (1) (2001) 249–264.

[21] A. Berezovski, Thermodynamic interpretation of finite volume algorithms, Journal of Structural Mechanics (Rakenteiden Mekaniikka) 44 (3) (2011) 156–171.

[22] A. L. McKelvey, R. O. Ritchie, On the temperature dependence of the superelastic strength and the prediction of the theoretical uniaxial transformation strain in nitinol, Philosophical Magazine A 80 (8) (2000) 1759–1768.

[23] J. Glimm, E. Isaacson, D. Marchesin, O. McBryan, Front tracking for hyperbolic systems, Advances in Applied Mathematics 2 (1) (1981) 91–119.

[24] N. Risebro, A. Tveito, A front tracking method for conservation laws in one dimension, Journal of Computational Physics 101 (1) (1992) 130–139.

[25] D.-K. Mao, A shock tracking technique based on conservation in one space dimension, SIAM Journal on Numerical Analysis 32 (5) (1995) 1677–1703.

[26] J. Glimm, X. L. Li, Y. Liu, N. Zhao, Conservative front tracking and level set algorithms, Proceedings of the National Academy of Sciences 98 (25) (2001) 14198–14201.

[27] C. Gatti-Bono, P. Colella, D. Trebotich, A second-order accurate conservative front-tracking method in one dimension, SIAM Journal on Scientific Computing 31 (6) (2010) 4795–4813.

[28] P. S. Rawat, X. Zhong, On high-order shock-fitting and front-tracking schemes for numerical simulation of shock–disturbance interactions, Journal of Computational Physics 229 (19) (2010) 6744–6780.